Electronic Supplementary Material (ESI) for Energy & Environmental Science.

Real-time Imaging of Activation and Degradation of Carbon Supported Octahedral Pt-Ni Alloy Fuel Cell Catalysts at the Nanoscale Using *in situ* Electrochemical Liquid Cell STEM

Vera Beermann, Megan E. Holtz, Elliot Padgett, Jorge Ferreira de Araujo, David A. Muller,* and Peter Strasser*

** Corresponding author email address: david.a.muller@cornell.edu* and *pstrasser@tu-berlin.de*

This PDF file includes:

Materials and Methods
Fig. S1 to S5
Captions for Movies S1 to S3

Other Supplementary Materials for this manuscript include:

Movies S1 to S3

Materials and Methods

Chemicals and Materials

Platinum(II)acetylacetonate ($Pt(acac)_2$, Pt 48% min.), nickel(II)acetylacetonate ($Ni(acac)_2$, 95.0 %), tungsten hexacarbonyl ($W(CO)_6$, 97.0 %) and oleic acid (OAc, 90 %) were obtained from Alfa Aesar. Oleylamine (OAm, 98.0 %) was obtained from Sigma Aldrich. All chemicals were used as received.

Synthesis of Pt-Ni Nanoparticles

We investigated ~8 nm octahedral Pt-Ni nanoparticles that exhibited an average composition of $Pt_{34}Ni_{66}$ and were supported on Vulcan XC 72R carbon supports. The synthesis of Pt-Ni/C octahedral nanoparticles was described earlier[1]. Shortly, $Pt(acac)_2$, $Ni(acac)_2$, OAm and OAc were stirred under nitrogen atmosphere at 60 °C for 10 min, followed by raising the temperature to 130 °C. $W(CO)_6$ was added rapidly, nitrogen purging was stopped and the reaction mixture was heated to 230 °C and then stirred for 50 minutes. After cooling down to RT toluene and ethanol (EtOH) were added to the reaction mixture. The supernatant was removed by centrifugation and re-dispersed in toluene. The dispersion was added to a dispersion of Vulcan XC 72R in toluene. The mixture was sonicated with an ultrasonic horn for 30 min. Afterwards EtOH was added and the catalyst was centrifuged, washed

with EtOH and freeze dried. In the subsequent annealing step the supported particles were heated with 10 K min^{-1} to 180 °C in a tube furnace in synthetic air atmosphere for 30 min. After purging nitrogen for 30 min the atmosphere was changed to hydrogen and the temperature was raised with 10 K min^{-1} to 300 °C for 1 h.

In situ TEM investigations

For TEM investigations a Protochips Poseidon electrochemical cell holder was used. The liquid flow cell portion[2,3] and the electrochemical cell design[4] has been discussed previously. The Pt-Ni catalyst nanoparticles were dispersed into isopropanol solution and drop cast onto the chips with electrodes after cleaning. The Pt-Ni catalyst was then dispensed on the carbon working electrode, as well as the platinum reference and counter electrodes. Because the reference and counter electrodes are made of platinum and are large compared to the dispersed nanoparticles, they should not affect electrode behavior. We initially flowed a solution of 0.1 M $HClO_4$ / H_2O (diluted from 70 % conc. $HClO_4$, 99.999 % trace metal bases, Sigma Aldrich with milli-Q water) into the cell at 300 µL/hr to wet most of the cell and then flowed solution at 50 µL/hr during the experiment using a syringe pump (Infuse/Withdraw Pump 11 Pico Plus Elite, Harvard Apparatus). In this particular experiment, there was a bubble over parts of the working electrode which was slowly pushed to the side over the course of the experiment, giving us fresh regions of the working electrode which had experienced no previous electrochemistry (resulting in the slow increase of total current measured over time from the electrode). The liquid was likely still flowing around the bubble, refreshing the solution over the course of the several-hour experiment. However, the solution chemistry still may change over the course of the experiment due to the irradiation of the electron beam[5] and the electrochemical treatments which were occurring in a small volume. To minimize changes in chemistry, we chronologically performed our experiments with the less severe degradation protocol and increasingly stepped up the potentials. To decouple the chemical effect, we performed control experiments to compare regions on the electrode to regions nearby which are off of the electrode, which experienced no electrochemistry. The electrolyte layer thickness was 300 nm, estimated by electron energy loss spectroscopy[2]. A “floating-type” Gamry potentiostat was used for the *in situ* TEM measurements. The platinum reference electrode was calibrated in 0.1 M perchloric acid using the well-known characteristics of the hydrogen underpotential deposition region of platinum-based materials, as shown in Figure 1d. With that,

0.0 V_{RHE} was correlated to -0.8 V_{Pt}. All potentials are reported against the reversible hydrogen electrode (RHE) based on this calibration to allow better comparability to literature.

In situ microscopy was performed using a monochromated FEI Tecnai F-20 STEM/TEM operated at 200 kV and equipped with a Gatan 865 HR-GIF spectrometer for EELS analysis. Electron beam conditions were selected to optimize imaging conditions while minimizing beam damage, ranging from 30 – 60 e^- / nm^2s for HAADF-STEM imaging with a 9.6 mrad convergence angle. During control experiments with no electrochemical biasing, we observed that a beam dose of 110 e^- / nm^2s induced damage while a dose around 60 e^- / nm^2s did not show significant change after 10 minutes of imaging. The dose reported is the averaged dose rate over the entire field of view: the probe current was varied between 2.6 and 4.9 pA using the monochromator while maintaining the 9.6 mrad probe. The 4.9 pA probe current was used at lower magnifications with a field of view of 1.01 microns, and the 2.6 pA probe current was used during imaging with a field of view of 517 nm. The number of pixels across all datasets was 512 and the dwell time was 12 us. For the movies in the supplemental material, denoising through imageJ was run to enhance signal to noise [6-8].

Ex situ TEM investigations

Ex situ imaging was performed using a monochromated FEI Titan Themis CryoS/TEM operated at 300 kV, with a 21.4 mrad convergence angle.

Ex situ Electrochemical Characterization

For *ex situ* electrochemical characterization a conventional three electrode cell with a Pt gauze as counter electrode (Pt furled Pt 5x5 cm^2 mesh), a reference electrode (MMS Hg/Hg_2SO_4 with the potential E= -0.723 V_{RHE}) and a glassy carbon working electrode (5 mm diameter) was used. The working electrode always was lowered into the electrolyte under potential control at +0.05 V_{RHE}. A 0.1 M $HClO_4$ was used for electrochemical measurements (diluted from 70 % conc. $HClO_4$, 99.999 % trace metal bases, Sigma Aldrich with milli-Q water). All measurements were performed with a BioLogics Science Instruments potentiostat SP-200. To prepare an ink 2.5 mg of catalyst were added into 2.5 mL water, 7 µL Nafion (5 wt%) and 0.5 mL isopropanol (≥ 99.5 %) and ultrasonicated for 15 minutes. 10 µL of the ink were placed on a glassy carbon rotating disk electrode, which results in a Pt loading of 6-7 µg cm^{-2}. The film was dried at 60 °C for 7 minutes.

Differential Electrochemical Mass Spectrometry (DEMS) measurements

Differential electrochemical mass spectrometry (DEMS) were recorded using a home designed dual thin-layer electrochemical flow cell partly based the original design reported elsewhere[9]. The gas products from the flow cell was detected using a Prisma™ quadrupole mass spectrometer (QMS 200, Pfeiffer-Vacuum) with two turbomolecular pumps (HiPace 80) operating under 10^{-6} mbar. The electrolyte was separated from the chamber by a 150 µm thick hydrophobic PTFE membrane (Cat. No. PF-003HS for Cobetter® porous size 30 nm). The working electrode has an exposed area of ~ 0.193 cm^2 and pressured against a Teflon gasket to form a thin layer with defined thickness around 100µm. A Pt-mesh was used as counter electrode connected to tangential channel to main inlet channel and real hydrogen reference electrode (RHE) to monetarize the potential. Measurements were recorded on a Biologic SP-200 potentiostat in 0.1 M $HClO_4$ (diluted from 70 % conc. $HClO_4$, 99.999 % trace metal bases, Sigma Aldrich with milli-Q water). Pt-Ni/C were homogenously dispersed by ultrasonication for 15 min, and drop-dried onto a pre-defined area ~ 0.193 cm^2 with inert Teflon film coated on glassy carbon electrodes (Φ = 10 mm in, HTW GmbH). The glassy carbon electrodes were polished with silica slurries (Buehler) of 1 µm and 0.05 µm in particle size and cleaned in acetone and milli-Q water. The electrolyte flow speed was set at the out let flow cell with a needle valve with 2µL s^{-1} and controlled during experiments with a liquid flow sensor Sensirion SLQ-QT500. Measurements done without any compensated for the ohmic resistance. The WE and Teflon gasket contact were purged with N_2 in order to avoid environment air into the reaction compartment or exchange with MS chamber. The cyclic voltammetry mass spectrometer (MSCV) curves were recorded during cycling form 0.05V_{RHE} with most anodic potential varying from 1.0 V_{RHE}, 1.2 V_{RHE} and 1.4 V_{RHE} at a scan-rate of 100mV s^{-1}, with four selective channels recording m/z 44 with electrochemical measurements. To assure optimized detection of products during potential cycling as assessed with mass spectrometer, the ion source was calibrated using calibration protocol presented at Quadera software. The background stability and reproducibility was achieved by baking of vacuum chamber and mass spectrum calibration prior to experimental DEMS measurements. The ionization was preformed with electron beam at 80 eV. The amplification of the secondary electron multiplier (SEM) was setup to be around 3 orders of magnitude higher with reference to Faraday detector.

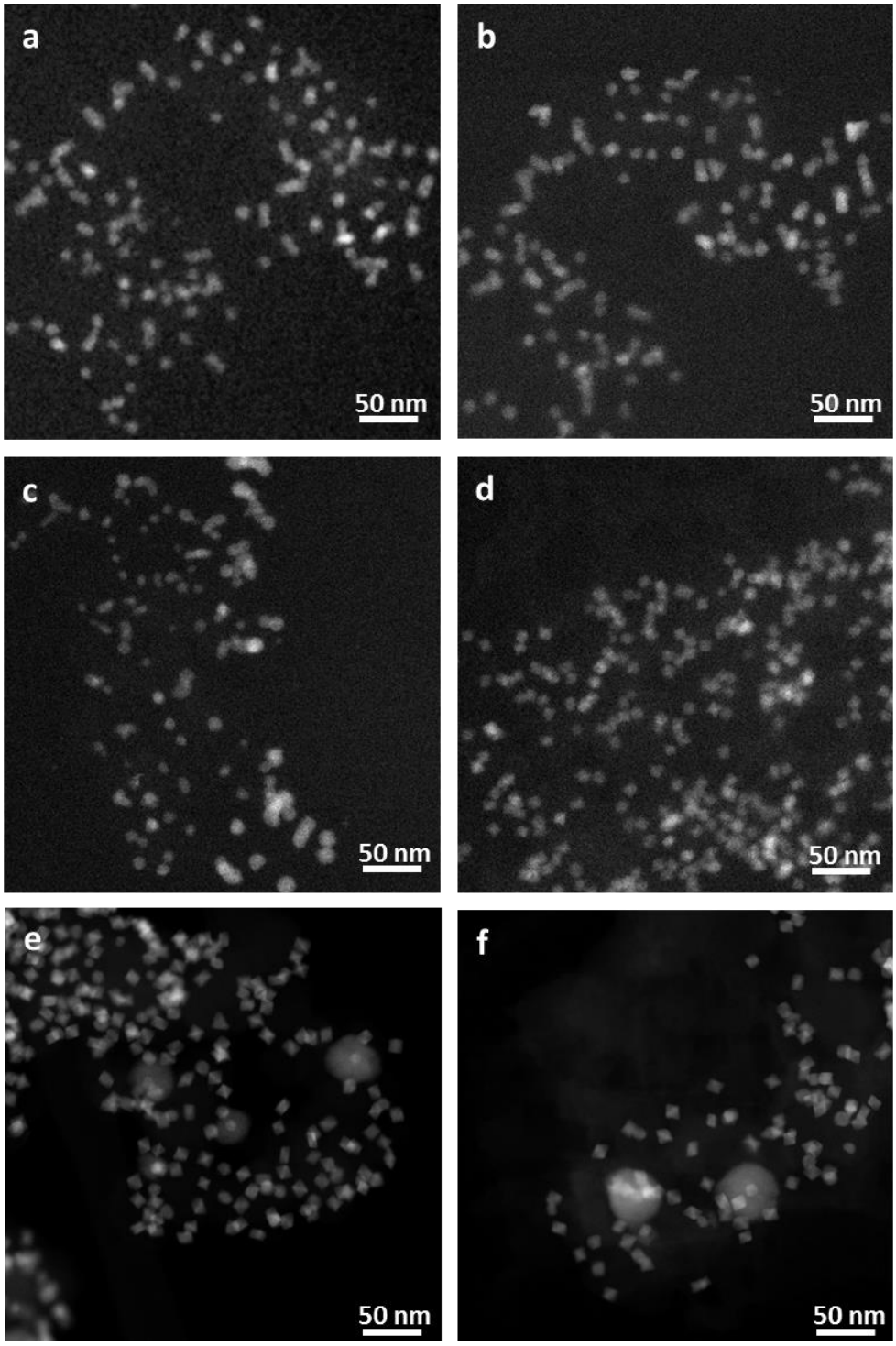

Figure S1 Comparisons of shape change with and without the electron beam. HAADF STEM images of particles before **a** and after **b** in situ cycling from 0 to +1.2 V_{RHE} with continual imaging. The carbon support bends during cycling and there is some coalescence leading to octahedral shape degradation. Images of the particles which are on **c** and off **d** the electrode in the in situ cell after cycling where neither region was exposed to the electron beam. Particles on the electrode show rounded surfaces and appear to be larger. Particles off the electrode maintain their octahedral shape and size. From this, we conclude that there were electrochemical effects on the particles on the electrode that cannot be accounted for by the electron beam or exposure to electrolyte alone. HAADF STEM images of the *ex situ* particles in an aberration corrected STEM before **e** and after **f** the same electrochemical procedure, showing significantly less shape change than the in situ experiment, although some shape change is observed.

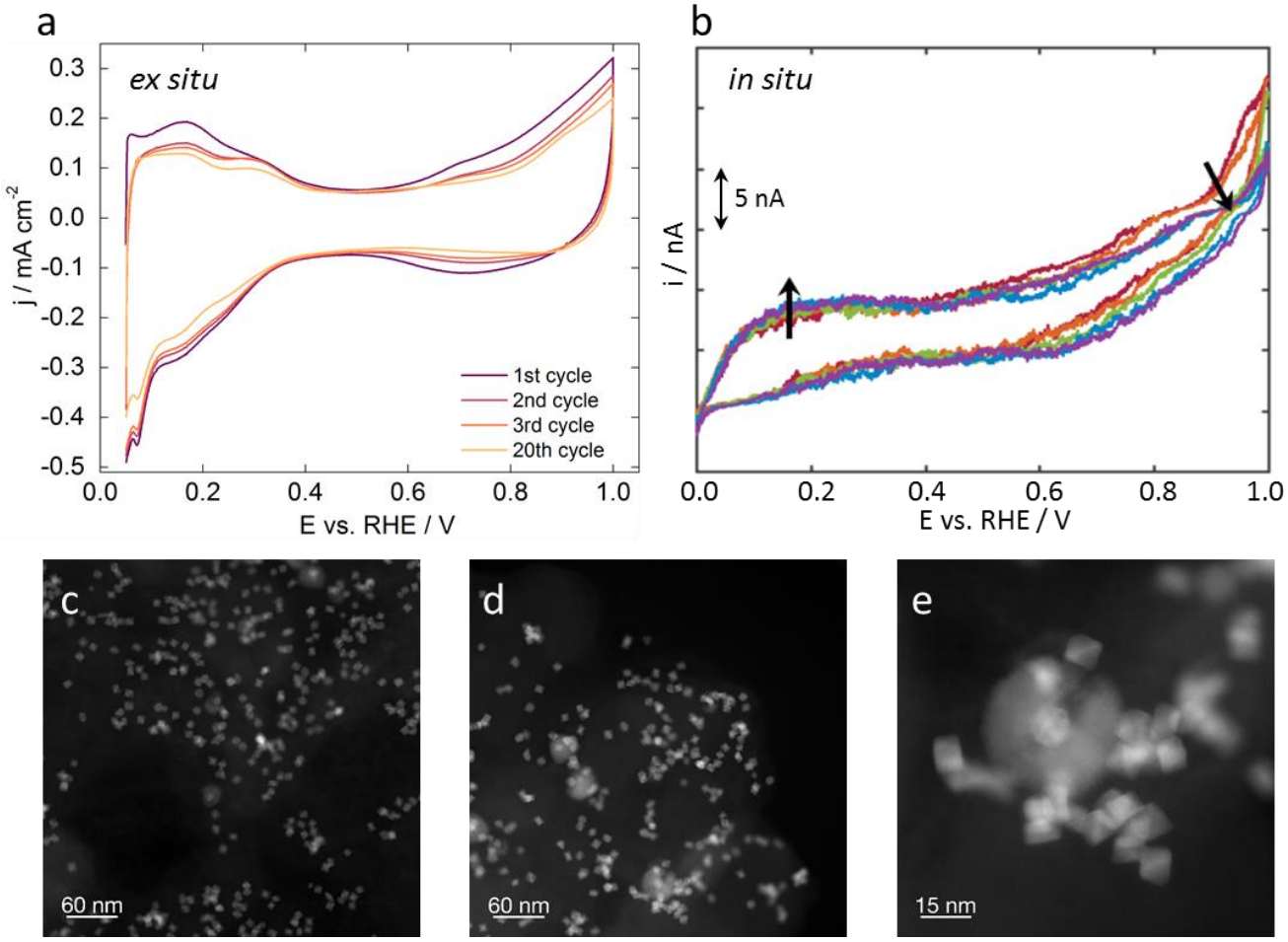

Figure S2 ***Ex situ*** **electrochemical data measured in a three electrode RDE setup** between **a** 0.05 – 1.0 V_{RHE}, 20 (+5) cycles, 100 mV s^{-1}, N_2 sat. 0.1 M $HClO_4$); **b** *In situ* electrochemical data measured in the protochips electrochemistry TEM holder (-0.8 – 0.2 V_{Pt}, 40 (+5) cycles, 100 mV s^{-1}, 0.1 M $HClO_4$); **c-d** HAADF images of the catalyst after similar ex situ electrochemical treatment. Ni-rich particles remain (as shown in d,e) but some show signs of the beginning of the dissolution process observed in situ. In these images, the octahedral shape of the Pt-Ni nanoparticles remains.

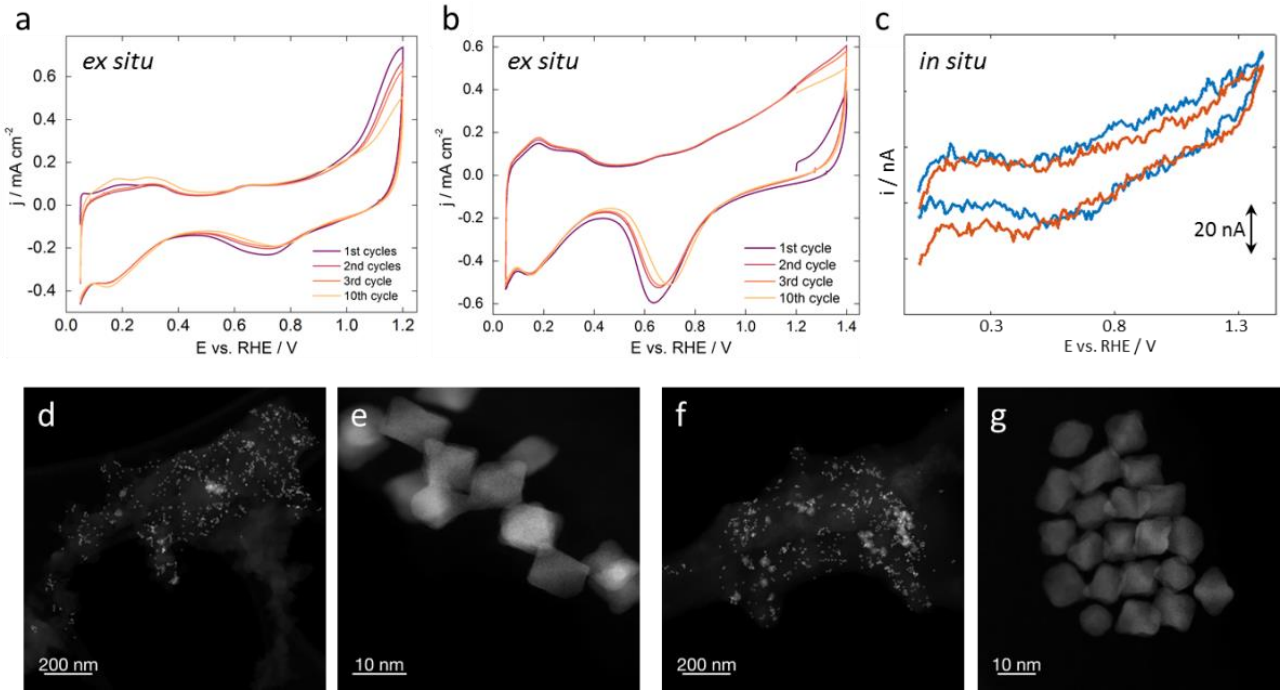

h

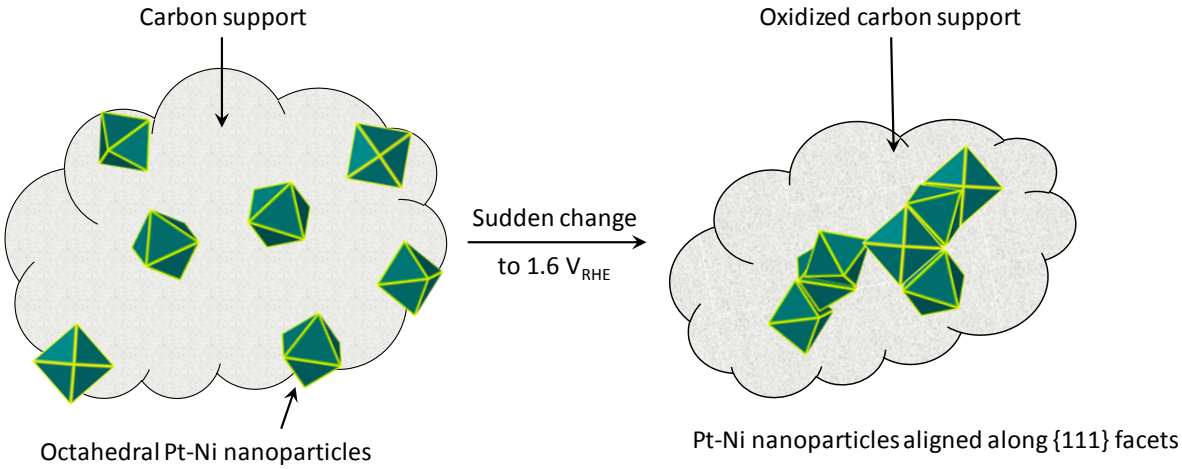

Figure S3 ***Ex situ*** **electrochemical data measured in a three electrode RDE setup** between **a** 0.05 – 1.2 V_{RHE} and **b** 0.05 – 1.4 V_{RHE}, 10 cycles, 100 mV s^{-1}, N_2 sat. 0.1 M $HClO_4$; **c** In situ electrochemical data measured in the protochips electrochemistry TEM holder (-0.8 – 0.6 V_{Pt}, 10 cycles, 100 mV s^{-1}, 0.1 M $HClO_4$); **d,e** HAADF images of the catalyst after ex situ electrochemical treatmed between 0.05 – 1.2 V_{RHE}; particle facets remain but may be beginning to soften **f,g** HAADF images of the catalyst after ex situ electrochemical treatmed between 0.05 – 1.4 V_{RHE}; faces of the particle are pulling in and the corners are more rounded. However, in both of these images, the particle shape hasn't changed as drastically as it did in the corresponding in situ experiment. **h**. Schematic illustration of the coalescence event happening after sudden changes in potential to 1.6 V_{RHE}. The carbon support is oxidized, causing a loss in the anchoring point for the Pt-Ni nanoparticles and results in particle agglomeration.

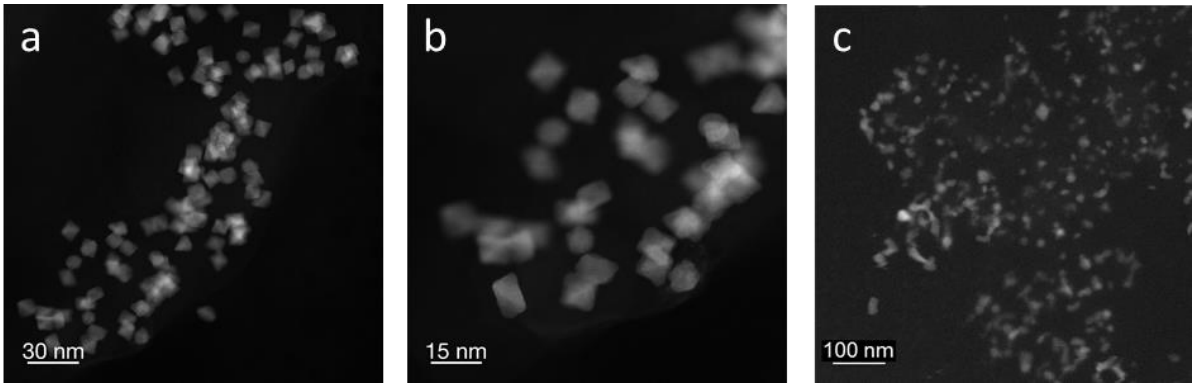

Figure S4 *Ex situ* HAADF STEM images. a, b HAADF STEM images of the catalyst after ex situ electrochemical treatment for 20 cycles and subsequent step into high potential of +1.4 V_{RHE} (100 mV s^{-1}, 0.05 – 1.2 V_{RHE}). The octahedral shape remains, and the particles do not show strong coalescence. **c** Image from the in situ cell, on other areas of the electrode which were not imaged during cycling, showing similar coarsening effects that were observed in the in situ imaged region.

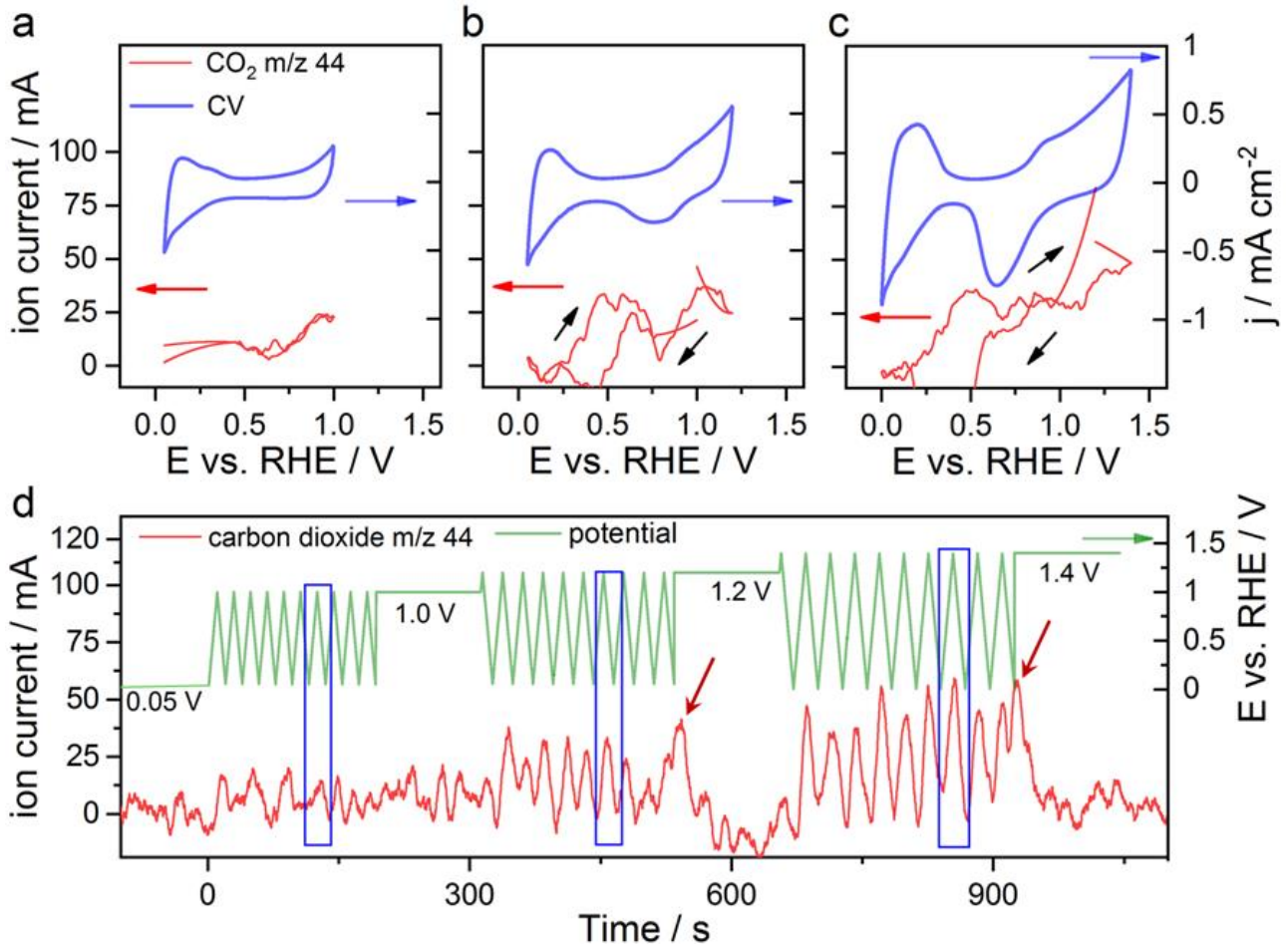

Figure S5 Simultaneously recorded of cyclic voltammograms (CV) and mass spectrometry cycle voltammograms (MSCV) during anodic potential step at dual thin-layer flow cell. a-c Ion current for carbon dioxide (m/z 44) evolution over electrochemical potential (V_{RHE}) at left side and the corresponding measured current densities normalized to the electrode area on the right side. R and blue arrows indicate the axis, black arrow the scan direction. **d** Variation of mass spectrum signal intensity m/z 44 over experimental time for each set of CVs and constant potential step shown on the left side and the corresponding potential shown on the right side, blue boxes indicate the region which were used to extract a-c. The electrochemical CVs on Pt-Ni/C was recorded in Ar sat. 0.1 M $HClO_4$ with 100mV s^{-1}. Measurements were done without any uncompensated ohmic resistance determined by electrochemical impedance spectroscopy. Green arrow indicate the axis.

Figure S5 represents detailed results from our Differential Electrochemical Mass Spectrocopy (DEMS) measurements. Figure S5a-c shows examples of the cyclic voltammograms with different upper potentials and the corresponding ion currents for carbon dioxide (CO_2). When cycling up to 1.0 V_{RHE} (Figure S5a) CO_2 was detected at a very low level which nearly equals the noise level and is still within the sensitivity of the mass spectra in the ppm range. Applying an upper potential of 1.2 V_{RHE} (Figure S5b) the values of the resulting ion currents nearly double, indicating an increased formation CO_2. At upper potentials of 1.4 V_{RHE} CO_2 shows an enormous increase in ion current intensity. From that we

conclude, that potentials of 1.2 and 1.4 V_{RHE} cause carbon corrosion, which of course is more severe at 1.4 V_{RHE}.

Figure S5d presents the variation of the mass spectrum signal during the overall applied potential sequence with the corresponding potentials as function of time. During hold at 0.05 V_{RHE} the ion current stays at noise level until cycling up to 1.2 V_{RHE} starts. When cycling up to 1.2 V_{RHE} the ion current nicely follows the changes in potential, indicating an increase in CO_2 production during anodic scans. When changing to a constant potential of 1.2 V_{RHE} a sudden increase of the CO_2 signal (highlighted by the red arrow) can be observed, which is in excellent agreement with our findings from Figure 3d,e and Movie 2. During hold at 1.2 V_{RHE} the CO_2 signal goes back to noise level again, indicating no further carbon corrosion. Cycling up to 1.4 V_{RHE} shows a nice connection between the potential and the ion current of both molecules again. In comparison to the previous one, the ion current intensity is higher, indicating a larger amount of CO_2 production and thus a higher degree of carbon corrosion, which is consistent with our discussion on the TEM movies (severe changes described for Figure 3h,i). Hold at 1.4 V_{RHE} causes again an increase in the CO_2 signal even though it is not as pronounced as for the hold at 1.2 V_{RHE}. For both transition to the constant potential hold however, the CO_2 signal goes back to static condition i.e. noise level. Again, this indicates and supports our statement from before, that most severe changes happening during the transition to a constant potential and that the constant potential itself does induce major changes in the catalyst.

Movie S1

HAADF STEM Movie of catalyst structure during electrochemical potential cycling between -0.8 and +0.2 V_{Pt} (0.0 and +1.0 V_{RHE}) in 0.1 M $HClO_4$ for 20 CV with 100 mV s^{-1} sweep rate and the corresponding animated potential profile over time.

Movie S2

HAADF STEM Movie of the impact on the catalyst structure of an electrochemical sequence consisting of electrochemical potential cycling between -0.8 to +0.4 V_{Pt} and -0.8 to +0.6 V_{Pt} (0.0 to +1.2 V_{RHE} and 0.0 to +1.4 V_{RHE}) for 10 CV with 100 mV s^{-1} and holding on different upper potentials in 0.1 M $HClO_4$ and the corresponding animated potential profile over time.

Movie S3

HAADF STEM Movie imaging of the catalyst structure during electrochemical potential cycling between -0.8 to +0.4 V_{Pt} (0.0 and +1.2 V_{RHE}) for 20 CV with 100 mV s^{-1} sweep rate, followed by a step into a high potential and the corresponding animated potential profile over time.

Literature

1 Beermann, V. *et al.* Tuning the Electrocatalytic Oxygen Reduction Reaction Activity and Stability of Shape-controlled Pt-Ni Nanoparticles by Thermal Annealing – Elucidating the Surface Atomic Structural and Compositional Changes. *Journal of the American Chemical Society*, doi:10.1021/jacs.7b06846 (2017).

2 Holtz, M. E., Yu, Y. C., Gao, J., Abruna, H. D. & Muller, D. A. In Situ Electron Energy-Loss Spectroscopy in Liquids. *Microscopy and Microanalysis* **19**, 1027-1035, doi:10.1017/S1431927613001505 (2013).

3 Klein, K. L., Anderson, I. M. & de Jonge, N. Transmission electron microscopy with a liquid flow cell. *J Microsc* **242**, 117-123, doi:10.1111/j.1365-2818.2010.03484.x (2011).

4 Holtz, M. E. *et al.* Nanoscale Imaging of Lithium Ion Distribution During In Situ Operation of Battery Electrode and Electrolyte. *Nano Letters* **14**, 1453-1459, doi:10.1021/nl404577c (2014).

5 Schneider, N. M. *et al.* Electron–Water Interactions and Implications for Liquid Cell Electron Microscopy. *The Journal of Physical Chemistry C* **118**, 22373-22382, doi:10.1021/jp507400n (2014).

6 Luisier, F., Vonesch, C., Blu, T. & Unser, M. Fast interscale wavelet denoising of Poisson-corrupted images. *Signal Processing* **90**, 415-427, doi:10.1016/j.sigpro.2009.07.009 (2010).

7 Luisier, F. The SURE-LET Approach to Image Denoising. *Swiss Federal Institute of Technology Lausanne - EPFL Thesis* **4566** (2010).

8 Luisier, F., Vonesch, C., Blu, T. & Unser, M. in *Biomedical Imaging: From Nano to Macro, 2009. ISBI'09. IEEE International Symposium on.* 310-313 (IEEE).

9 Jusys, Z., Massong, H. & Baltruschat, H. A new approach for simultaneous DEMS and EQCM: Electro-oxidation of adsorbed CO on Pt and Pt-Ru. *J. Electrochem. Soc.* **146**, 1093-1098, doi:10.1149/1.1391726 (1999).